Nanostructured materials with highly dispersed Au–$Ce_{0.5}Zr_{0.5}O_2$ nanodomains: A route to temperature stable Au catalysts?

Jean-Yves Chane-Ching,*[a] Florian Moncho,[a] Dimitri Truyen,[a] Pierre Alphonse,[a] Christophe Tenailleau,[a] Jean-Daniel Marty[b] and Lucien Datas[a]

DOI: 10.1039/b805397a

Our strategy to inhibit Au(0) growth with temperature involves the preparation of ultrafine Au clusters that are highly dispersed and strongly interacting with a thermally stable high-surface-area substrate. Temperature-stable Au-cluster-based catalysts were successfully prepared through the controlled synthesis of 3.5 nm $Ce_{0.5}Zr_{0.5}O_2$ colloidal building blocks containing tailored strongly bound Au-cluster precursors. With the objective of stabilizing these Au clusters with temperature, grain growth of $Ce_{0.5}Zr_{0.5}O_2$ nanodomains was inhibited by their dispersion through Al_2O_3 nanodomains. High surface area Au–$Ce_{0.5}Zr_{0.5}O_2$–Al_2O_3 nanostructured composites were thus designed highlighting the drastic effect of Au cluster dispersion on Au(0) cluster growth. High thermal stability of our Au(0)-cluster-based catalysts was shown with the surprising catalytic activity for CO conversion observed on our nanostructured materials heated to temperatures as high as 800 °C for 6 h.

Introduction

Gold clusters supported on metal oxide substrates have received considerable attention experimentally and theoretically for improving the activity for a number of applications including solar energy conversion,[1] low-temperature oxidation of carbon monoxide (CO),[2,3] selective CO oxidation in fuel cells,[4] direct synthesis of hydrogen peroxide[5] and production of vinyl acetate monomers.[6,7] Gold is typically used at low or moderate temperatures since Au clusters are known to exhibit fast coarsening and sintering at high temperatures. Indeed, the development of heat-stable Au-based catalysts[8] represents a true challenge and will offer new opportunities for Au cluster catalysis if innovative routes to Au cluster stabilization at high temperatures are proposed.[9] A first area of opportunity concerns the automotive industry where low-temperature start up performance of catalysts remains an area in which improvement is sought.[9] Since the temperature required for oxidation of hydrocarbons is about 300 °C, with peak temperatures around 800 °C, thermal durability of gold-based catalysts must be improved for the future development of such a promising market.[10] A second area of application may involve catalytic reactions where selectivity is required. For instance, achievement of Au-catalyst, pre-heat treated at high temperature should favour a catalyst comprising small gold particles whilst ensuring that all cationic gold is removed, a recently reported key factor to control the activity and selectivity for preferential oxidation reactions.[4] Lastly, there is another area of applications where considerable effort has been devoted to the design of heat-stable Au-based catalysts[8,11] with the objective to re-use the catalysts without loss of performance, it concerns Au-catalysts displaying long-term catalytic activity.

To the best of our knowledge, few articles[12–14] describe high-temperature stable Au-catalysts. A first strategy was proposed for catalysts developed for the direct epoxidation of propene at 400 °C.[12] The enhanced stability compared with the classical Au-cluster–TiO_2 catalysts has been achieved by dispersing Au clusters on a high-surface-area and temperature-stable TS_1 silicalite, a titanium-containing support. More recently, another strategy for the stabilization of Au nanoparticles against sintering was proposed involving isolation of Au metal catalyst particles *via* hollow sphere encapsulation. These catalysts are composed of ZrO_2[13] or SnO_2[14] inorganic oxide shells with exactly one gold nanoparticle in each shell. Nevertheless, this process route is reported as rather expensive and time consuming.[13]

Our strategy to inhibit Au(0) growth first involves the preparation of ultrafine Au clusters that are highly dispersed and strongly interacting with a thermally stable high-surface-area substrate. For catalytic purposes, the characteristics of the metal oxide surface support are of paramount importance. Oxides such as Fe_2O_3, TiO_2 and CeO_2, have been shown to be appropriate,[15–17] especially in the form of discrete nanosized particles.[18] For instance, well defined nanocrystalline CeO_2 particles increase the Au activity for CO conversion due to modification of surface electronic properties when the particle size is decreased to the nanoscale. Since the addition of the ZrO_2 component is known to increase the thermal stability of CeO_2[19] we selected $Ce_{0.5}Zr_{0.5}O_2$ as the substrate and thus prepared 3.5 nm $Ce_{0.5}Zr_{0.5}O_2$ individualized colloidal building blocks containing highly homogeneously distributed Au. With the objective of stabilizing these Au clusters with temperature, grain growth of $Ce_{0.5}Zr_{0.5}O_2$ nanodomains was inhibited by their dispersion through Al_2O_3 nanodomains. Indeed, the Al_2O_3 nanodomain was selected since as a carrier Al_2O_3[20,21] is well known to stabilize noble metal clusters *via* the formation of $Ce_{0.5}Zr_{0.5}O_2$–Al_2O_3

[a]*CIRIMAT, CNRS, Université de Toulouse, 118 Route de Narbonne, 31062 Toulouse, France. E-mail: chane@chimie.ups-tlse.fr*
[b]*IMRCP, Université de Toulouse, 118 Route de Narbonne, 31062 Toulouse, France*

high-surface-area composite materials.[22] Manipulation of these nanocomposites using tailored Au–$Ce_{0.5}Zr_{0.5}O_2$ nanoparticle building blocks allowed us to determine the respective contributions of crucial parameters such as Au–$Ce_{0.5}Zr_{0.5}O_2$ inter nanoparticle distance, denoted $d_{CeZr-CeZr}$ and inter Au-cluster distance, d_{Au-Au} on Au cluster growth and sintering. High thermal stability of our Au(0)-cluster-based catalysts was shown with the surprising catalytic activity for CO conversion observed on our nanostructured materials heated to temperatures as high as 800 °C for 6 h.

Results and discussion

Au–$Ce_{0.5}Zr_{0.5}O_2$ building blocks

Au–$Ce_{0.5}Zr_{0.5}O_2$ building blocks were synthesized using an aqueous route based on the hydroxide co-precipitation of a solution containing Ce(IV), Zr(IV) and Au(III) salts followed by re-dispersion in controlled acidic aqueous medium. Acetic acid was, for the first time, selected to minimize $Au(OH)_3$ dissolution during the acid-redispersion step. In contrast to conventional procedures that involve surface deposition of preformed Au(0) clusters on $Ce_{0.5}Zr_{0.5}O_2$ colloids, our co-precipitation synthetic route should favour incrustation of Au patches into the $Ce_{0.5}Zr_{0.5}O_2$ substrates. A large range of highly concentrated Au–$Ce_{0.5}Zr_{0.5}O_2$ coloured colloidal dispersions, with Au concentrations as high as 2 g l^{-1}, which are stable towards precipitation for over 6 months, were prepared with various weight ratios of Au, $x = (Au/Ce_{0.5}Zr_{0.5}O_2)_{wt}$, $0.002 < x < 0.05$. These proportions were determined by chemical analysis of the colloidal dispersions after their purification in ultra-filtration cells equipped with 3kDa, membranes. Transmission electron microscopy (TEM) performed on the purified dispersions revealed a nearly monodisperse size distribution of individualized colloids displaying an average size of ~3.5 nm and well crystallized domains, identified as $Ce_{0.5}Zr_{0.5}O_2$. EDS (X-ray energy dispersive spectroscopy) analysis performed on ~ 5 nm × 5 nm domains of individualized nanoparticle assemblies also showed the presence of Au, with x values consistent with chemical analysis. TEM investigations showed that the Au domains were generally fully attached to the $Ce_{0.5}Zr_{0.5}O_2$ nanoparticles with a gold particle diameter (d_{Au}) of < 3.5 nm (Fig. 1a). Closer inspection of the TEM images did not show the presence of any finer particles, but revealed a second population of nanoparticles, at very low concentrations (< 0.1% in number), displaying stronger contrast with size in the range of 4–6 nm (Fig. 1b). These larger and higher contrast nanoparticles were clearly identified by EDS as Au nanoparticles attached to $Ce_{0.5}Zr_{0.5}O_2$ nanoparticles. Evidence of the presence of Au(0) in the colloidal dispersions was demonstrated on the UV-Vis absorption spectra performed on the Au–$Ce_{0.5}Zr_{0.5}O_2$ coloured colloidal dispersions (Fig. 2). Indeed, the presence of Au(0) could be ascribed to the photo-reduction of Au(III) with H_2O under daylight UV excitation.[23] A main surface-plasmon band with 530 nm < l_1^{max} < 550 nm was observed for the various Au–$Ce_{0.5}Zr_{0.5}O_2$ colloidal dispersions and attributed to the plasmon resonance[24] of large Au(0) nanoparticles (> 2.5 nm). Since the dispersions possess high Au concentrations, the observation of this plasmon band originates from a very low number of large Au(0) nanoparticles. These large Au nanoparticles were determined to be < 0.1% in number from the UV absorbance values of the dispersions. This was confirmed by TEM observation. The ultrafine size of the Au(0) clusters was demonstrated from the UV-Vis spectra recorded on the dispersions after centrifugation at 4000 rpm. On these spectra, the shoulder observed at 500 nm is characteristic of a surface pre-plasmon band, usually ascribed to Au(0) clusters of size < 2 nm.[25,26] An increase in the proportion of these Au(0) clusters was achieved by synthesis at higher Au–$Ce_{0.5}Zr_{0.5}O_2$ contents, as shown by the higher intensity of the pre-plasmon band (see insert in Fig. 2). These observations indicate a highly homogeneous distribution of Au species in the Au–$Ce_{0.5}Zr_{0.5}O_2$ colloids, resulting in the formation of well individualized ultrafine Au(0) clusters under reductive conditions. Indeed, at this stage, a difference of colour was observed between as-prepared and $NaBH_4$-reduced dispersions revealing the presence of non-reduced Au^{3+} initially

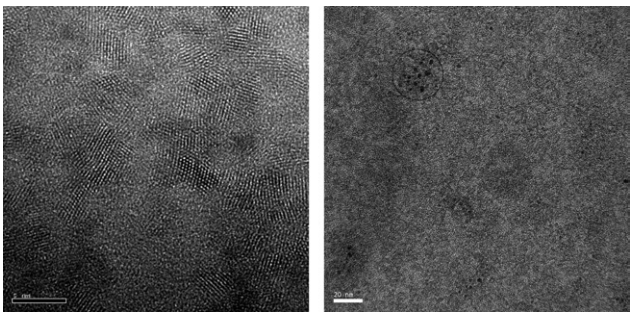

Fig. 1 a) HRTEM image of xAu–$Ce_{0.5}Zr_{0.5}O_2$, $x = 0.0215$, as-prepared colloidal dispersion showing well crystallized 3.5 nm average in diameter $Ce_{0.5}Zr_{0.5}O_2$ domains. Scale bar represents 5 nm. b) HRTEM of xAu–$Ce_{0.5}Zr_{0.5}O_2$, $x = 0.03$, colloidal dispersions showing a nearly monodisperse population of 3.5 nm Au–$Ce_{0.5}Zr_{0.5}O_2$ nanoparticles. Larger, 5 nm Au–$Ce_{0.5}Zr_{0.5}O_2$ nanoparticles are also observed. See ringed area. Scale bar represents 20 nm.

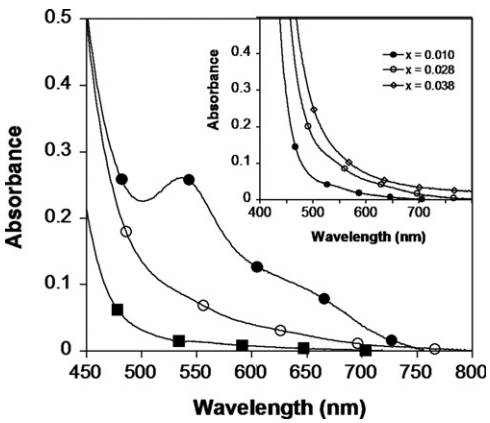

Fig. 2 UV-Vis spectra of colloidal dispersions demonstrating the presence of Au(0) clusters on xAu–$Ce_{0.5}Zr_{0.5}O_2$, $x = 0.028$, nanoparticle surfaces before (filled circles) and after centrifugation (open circles) at 4000 rpm. UV-Vis spectrum of $Ce_{0.5}Zr_{0.5}O_2$ dispersion without Au incorporation is given for reference (filled squares). Insert: UV spectra of Au–$CeZrO_2$ colloidal dispersions recorded after centrifugation showing an increase of the pre-plasmon band intensity with Au content in the dispersions.

precipitated within the Au–$Ce_{0.5}Zr_{0.5}O_2$ colloids but fully available to subsequently form Au (0) clusters. In the following, we used as-prepared Au–$Ce_{0.5}Zr_{0.5}O_2$ dispersions since preliminary comparative experiments with centrifuged dispersions did not show any differences in results resulting from the presence of the very low concentration of the large Au(0) nanoparticles.

Au–$Ce_{0.5}Zr_{0.5}O_2$–Al_2O_3 nanocomposites

The $Ce_{0.5}Zr_{0.5}O_2$–Al_2O_3 nanocomposites were prepared by incorporation of $Al(OH)_3$ building blocks, yielding Al_2O_3 nanodomains, to the Au–$Ce_{0.5}Zr_{0.5}O_2$ dispersions (Fig. 3). The effects of Au–$Ce_{0.5}Zr_{0.5}O_2$ inter-nanoparticle distances, $d_{CeZr-CeZr,}$ and of Au inter-cluster distances, d_{Au-Au} were investigated on materials prepared at similar Au weight concentrations, $y = ((Au)/(Al(OH)_3 + Ce_{0.5}Zr_{0.5}O_2))_{wt}$, but using Au–$Ce_{0.5}Zr_{0.5}O_2$ colloids having various Au contents (Fig. 4). To avoid homo-flocculation and rapid growth of Au–$Ce_{0.5}Zr_{0.5}O_2$ domains, we developed a nanoparticle assembly route, in a highly repulsive interaction regime both for Au–$Ce_{0.5}Zr_{0.5}O_2$ and $Al(OH)_3$ colloids. After drying of the product, this approach yielded randomly distributed Au–$Ce_{0.5}Zr_{0.5}O_2$ and $Al(OH)_3$ nanodomains. In a second step, our nanoparticle assembly process also included a re-dispersion stage with subsequent fast kinetic re-arrangement. This was achieved by dispersion-flocculation in alkaline medium (pH ~10 with NH_3) of the randomly distributed nanoparticle assembly after pre-consolidation by heat treatment for 6 h at 200 °C. This two-stage process was shown to significantly decrease the packing density of the nanoparticle assembly, as shown by pore-volume determination on materials calcined at 500 °C, yielding a large pore population centred around 6 nm while maintaining the local homogeneous distribution of the $Ce_{0.5}Zr_{0.5}O_2$ and $Al(OH)_3$ nanoparticles. Using this assembly process, high surface areas of up to ~ 70 m^2g^{-1} were reached on the nanocomposite samples after calcination for 6 h at 800 °C. The post-treatment with NH_4OH also allows

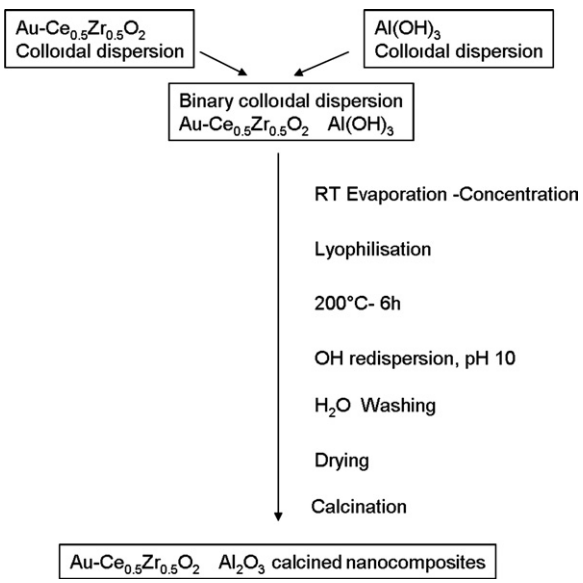

Fig. 3 Procedure for the preparation of Au–$Ce_{0.5}Zr_{0.5}O_2$–Al_2O_3 calcined nanocomposites.

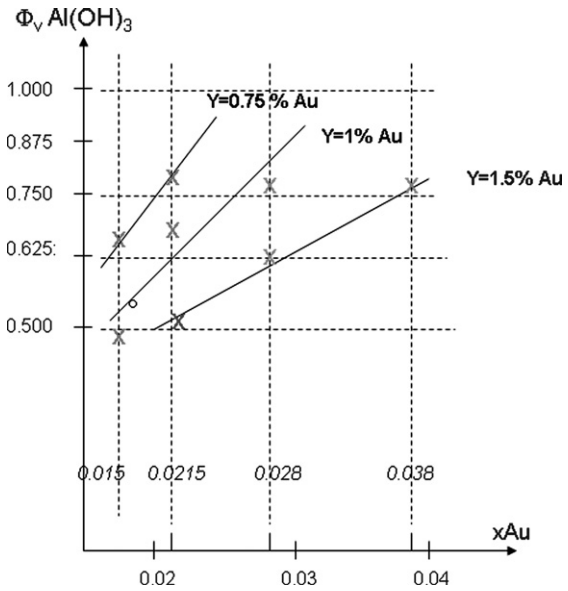

Fig. 4 $Al(OH)_3$ volume fractions in the nanocomposites prepared at y = 0.75, 1, and 1.5%, y = Au weight ratio in the nanocomposites. x_{Au} denotes the Au weight fraction in the Au–$Ce_{0.5}Zr_{0.5}O_2$ colloidal building blocks. Respective volume fractions of $Al(OH)_3$ and Au–$Ce_{0.5}Zr_{0.5}O_2$ building blocks were determined from mass and theoretical density of the corresponding (oxy)hydroxides. Mass of the Au–$Ce_{0.5}Zr_{0.5}O_2$ building blocks is determined from x and y values.

elimination of residual chloride from the Au clusters, a condition required for the inhibition of Au(0) cluster growth as previously reported by several authors.[2] Beneficial use of the $Al(OH)_3$ nanodomains to promote growth inhibition of $Ce_{0.5}Zr_{0.5}O_2$ domains was clearly demonstrated by XRD investigations performed on the Au–$Ce_{0.5}Zr_{0.5}O_2$–Al_2O_3 nanomaterials calcined for 6 h at 800 °C (Fig. 5). Consistently with an HRTEM inspection of the nanomaterials, $Ce_{0.5}Zr_{0.5}O_2$ crystallite sizes of 4.5 nm, slightly larger compared with $Ce_{0.5}Zr_{0.5}O_2$ colloidal building blocks were determined using Debye–Scherrer method after calcinations at 800 °C for the Au–$Ce_{0.5}Zr_{0.5}O_2$–Al_2O_3 nanocomposites prepared with Au–$Ce_{0.5}Zr_{0.5}O_2$ volume fraction of ~0.5. In contrast, a 10 nm domain size and surface area of ~ 22 m^2 g^{-1} were determined on pure Au–$Ce_{0.5}Zr_{0.5}O_2$ materials prepared without using $Al(OH)_3$ building blocks and calcined under similar conditions.

During these heat treatments in air, residual Au(III) species probably present as $Au(OH)_3$ in the $Ce_{0.5}Zr_{0.5}O_2$ domains became converted into Au(0) clusters. Growth and sintering of the whole population of Au(0) clusters, including previously described Au(0) clusters formed by photo-reduction, were investigated using TEM and XRD techniques on the various nanocomposites with y = 0.75, 1 and 1.5 Au wt%. For composites calcined 6 h at 800 °C and prepared from high Au content $Ce_{0.5}Zr_{0.5}O_2$ colloids, $x > 0.025$, characteristic peaks corresponding to Au(0) were observed on all the XRD patterns, whatever the Al_2O_3 content of the composites. In contrast, XRD patterns obtained from $y = 1$ and 1.5% Au composites, prepared from low Au content $Ce_{0.5}Zr_{0.5}O_2$ colloids, $0.002 < x < 0.025$, clearly display a lower growth of the Au(0) clusters. These observations highlight the drastic effect of Au inter-cluster

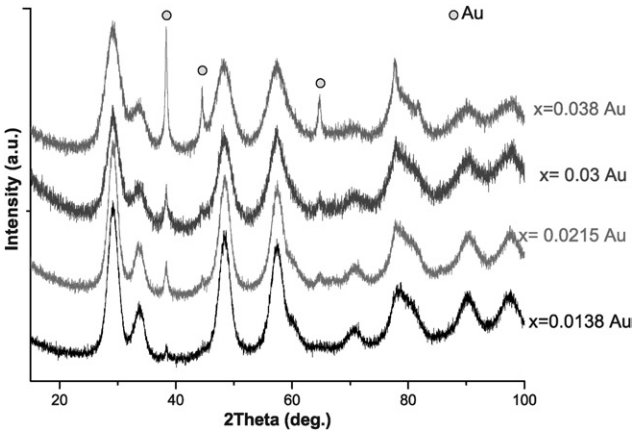

Fig. 5 XRD patterns of xAu–$Ce_{0.5}Zr_{0.5}O_2/Al_2O_3$ nanocomposites, calcined at 800 °C and prepared at same Au global content, $y = 1.5\%$, using xAu–$Ce_{0.5}Zr_{0.5}O_2$ colloids with various Au content, $0.0138 < x < 0.038$. Growth inhibition of $Ce_{0.5}Zr_{0.5}O_2$ domain is clearly observed with increase of x (or $\Phi v_{Al(OH)3}$) value. Increase of Au(0) crystallite size is observed with large x values, demonstrating more dramatic effect of $d_{Au–Au}$ compared with $d_{CeZr–CeZr}$ on Au cluster growth. Note that any peak attributed to Al_2O_3 could be observed highlighting the amorphous character of Al_2O_3 nanodomains in composites calcined at 800 °C.

distance, $d_{Au–Au}$, on Au(0) cluster growth compared with the Au–$Ce_{0.5}Zr_{0.5}O_2$ inter-colloid distance, $d_{CeZr–CeZr}$. The decrease of Au cluster growth and sintering with temperature using Au–$Ce_{0.5}Zr_{0.5}O_2$ building blocks with optimum Au content, $x = 0.0215$, was confirmed by high resolution transmission electron microscopy (HRTEM) investigation. Calcined nanocomposites reduced using 10 vol% H_2 in argon at 500 °C clearly show a fine regular nanostructure consisting of well crystallized nanodomains with sizes as small as <5 nm. EDS chemical analysis performed on these nanodomains using a 5.0 × 5.0 nm probe showed the presence of Ce, Zr and Au. This demonstrates that our route involving homogeneous Au precipitation in the $Ce_{0.5}Zr_{0.5}O_2$ nanodomains randomly dispersed among $Al(OH)_3$ particles yielded stable Au(0) clusters sized <5 nm after heat treatment at temperatures up to 500 °C. After calcination at $T = 800$ °C, a few larger Au particles with diameters up to 10 nm were observed (Fig. 6a). A more detailed TEM investigation of the nanocomposites also clearly revealed the presence of finer Au(0)

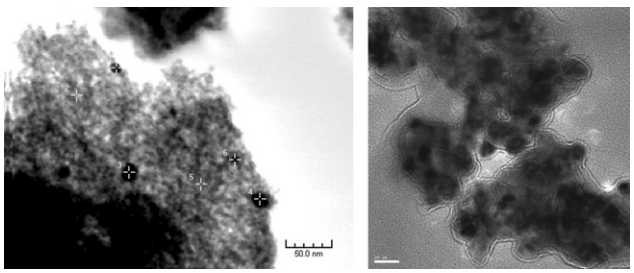

Fig. 6 a) TEM image of 6 h, 800 °C calcined xAu–$Ce_{0.5}Zr_{0.5}O_2$–Al_2O_3 nanomaterials, $x = 0.0215$, $y = 1.5$wt%. EDS analysis performed on various high-contrast areas, showed the presence of Au. Au nanoparticles sizes range from 5 to 20 nm b) TEM image of 6 h, 800 °C calcined Au–$Ce_{0.5}Zr_{0.5}O_2$ reference materials, $y = 1.5$ wt% showing Au nanoparticles with diameters ranging from 20 to 40 nm.

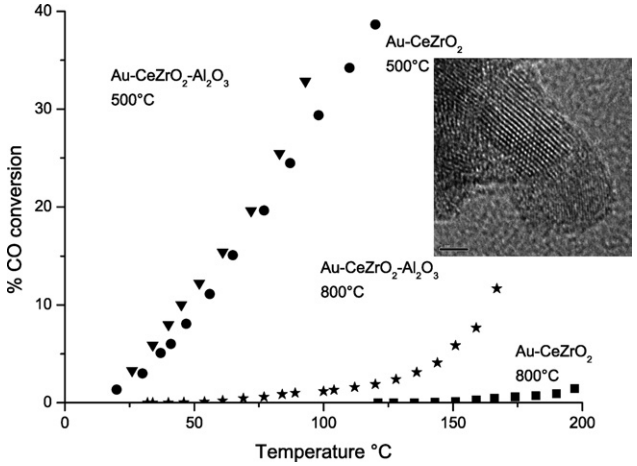

Fig. 7 Catalytic activities of pure Au–$Ce_{0.5}Zr_{0.5}O_2$ materials and Au–$Ce_{0.5}Zr_{0.5}O_2$–Al_2O_3 nanocomposites with identical Au contents, $y = 1.5\%$. a) Similar CO conversion rates were observed for materials calcined at 500 °C b) Higher CO conversion rates were achieved on Au–$Ce_{0.5}Zr_{0.5}O_2$–Al_2O_3 nanomaterials compared with pure Au–$Ce_{0.5}Zr_{0.5}O_2$ materials after calcination at 800 °C for 6 h. Insert: HRTEM image of Au–$Ce_{0.5}Zr_{0.5}O_2$–Al_2O_3 nanocomposite after calcination at 800 °C, 6 h showing two attached nanoparticles exhibiting inter-reticular distances of 0.30 nm and 0.21 nm corresponding to slightly titled (111) planes of $Ce_{0.5}Zr_{0.5}O_2$ and gold domains, respectively.

nanodomains, 4.5 nm attached to $Ce_{0.5}Zr_{0.5}O_2$ domains. As an illustration, Fig. 7 shows two attached nanocrystals with inter-reticular distances corresponding to the [111] planes of $Ce_{0.5}Zr_{0.5}O_2$ and Au(0), consistent with previous attributions reported by Akita *et al.*[27] Another interesting feature is the lower Au(0) cluster growth of our nanomaterials compared with Au 1.5 wt%–$Ce_{0.5}Zr_{0.5}O_2$ materials reference samples synthesized by surface deposition of preformed Au(0) clusters following a procedure previously described in the literature,[18] (Fig. 6b). This lower Au cluster growth probably originates both from the high surface area of our nanocomposites, and from stronger interactions between the $Ce_{0.5}Zr_{0.5}O_2$ surface and the Au(0) clusters. Indeed, our process route favours a deeper incrustation of the Au(0) clusters into the Au–$Ce_{0.5}Zr_{0.5}O_2$ nanoparticles compared with samples prepared from the standard Au cluster surface re-deposition process.

Catalytic activity of 800 °C, calcined Au–$Ce_{0.5}Zr_{0.5}O_2$–Al_2O_3 nanocomposites

To illustrate the thermal stability of the Au–$Ce_{0.5}Zr_{0.5}O_2$–Al_2O_3 nanocomposites, we investigated the catalytic activity of materials calcined at temperatures as high as 800 °C using CO conversion catalytic tests, performed from room temperature to 200 °C. For materials calcined at 500 °C, similar CO conversion rates were determined both on nanocomposites and Au–$Ce_{0.5}Zr_{0.5}O_2$ pure reference materials prepared with $y = 1.5$ Au wt%. After calcination at 800 °C for 6 h, as expected, no catalytic activity was observed for Au–$Ce_{0.5}Zr_{0.5}O_2$, $y = 1.5\%$, pure materials. In contrast, conversion rates of up to 30% were determined on Au–$Ce_{0.5}Zr_{0.5}O_2$–Al_2O_3 nanocomposites calcined for 6 h at 800 °C (Fig. 7) prepared using Au–$Ce_{0.5}Zr_{0.5}O_2$ colloids

with $x = 0.0215$. The improved catalytic activity of the nanomaterials is attributed to the presence of the very small ~4.5 nm Au nanocrystals as observed by HRTEM (Fig. 7).

Discussion

To the best of our knowledge, catalytic activity has never been reported for Au(0)-based catalysts calcined at temperatures as high as 800 °C. One key step for achieving enhanced temperature stability of the Au clusters is the controlled synthesis of 3.5 nm well dispersed $Ce_{0.5}Zr_{0.5}O_2$ building blocks containing tailored strongly bound Au cluster precursors. This enabled us to manipulate the inter-Au cluster distance, d_{Au-Au} and more importantly, cluster size by controlling the Au concentration of the Au–$Ce_{0.5}Zr_{0.5}O_2$ building blocks. Nanostructured composites using these Au–$Ce_{0.5}Zr_{0.5}O_2$ nanoparticles, juxtaposed with Al_2O_3 nanodomains were designed to yield highly thermal stable nanocomposites displaying minimal grain growth. We believe that the significant decrease of Au cluster sintering and coarsening, observed with temperatures as high as 800 °C, originate both from the successful inhibition of grain growth of the $Ce_{0.5}Zr_{0.5}O_2$ nanodomains (Fig. 8) and from an enhancement of the Au cluster–$CeZrO_2$ substrate interaction. Indeed, interaction between the Au clusters and $CeZrO_2$ nanodomains is probably strengthened using the co-precipitation route that we have developed for the synthesis of Au–$Ce_{0.5}Zr_{0.5}O_2$ building blocks, leading first to the formation of well distributed and well inserted ultrafine $Au(OH)_3$ domains that are subsequently converted into well-anchored Au clusters. From our results, we also highlight the crucial importance of dispersing a higher number of small clusters of well defined size rather than designing nanocomposites using Au–$Ce_{0.5}Zr_{0.5}O_2$ building blocks with larger Au cluster concentration and larger inter-Au cluster distance.

Conclusion

An increase of CO conversion by 15 fold was achieved on the resulting Au–$Ce_{0.5}Zr_{0.5}O_2$–Al_2O_3 nanocomposites compared with Au–CeO_2 nanomaterials reported elsewhere,[18] Further enhancement of catalytic activity of Au(0) clusters inserted into nanocomposites surfaces will be investigated by dispersing Au–$Ce_{0.5}Zr_{0.5}O_2$ building blocks into higher surface area substrates, *ca.* >300 $m^2\ g^{-1}$.[28] These high-temperature-stable Au(0)-based nanocomposites should open interesting routes in the field of high-temperature Au catalysis.

Experimental

*x*Au–$Ce_{0.5}Zr_{0.5}O_2$ (*x* wt% ranging from 0.002 to 0.05) colloidal dispersions were prepared by a modified procedure previously

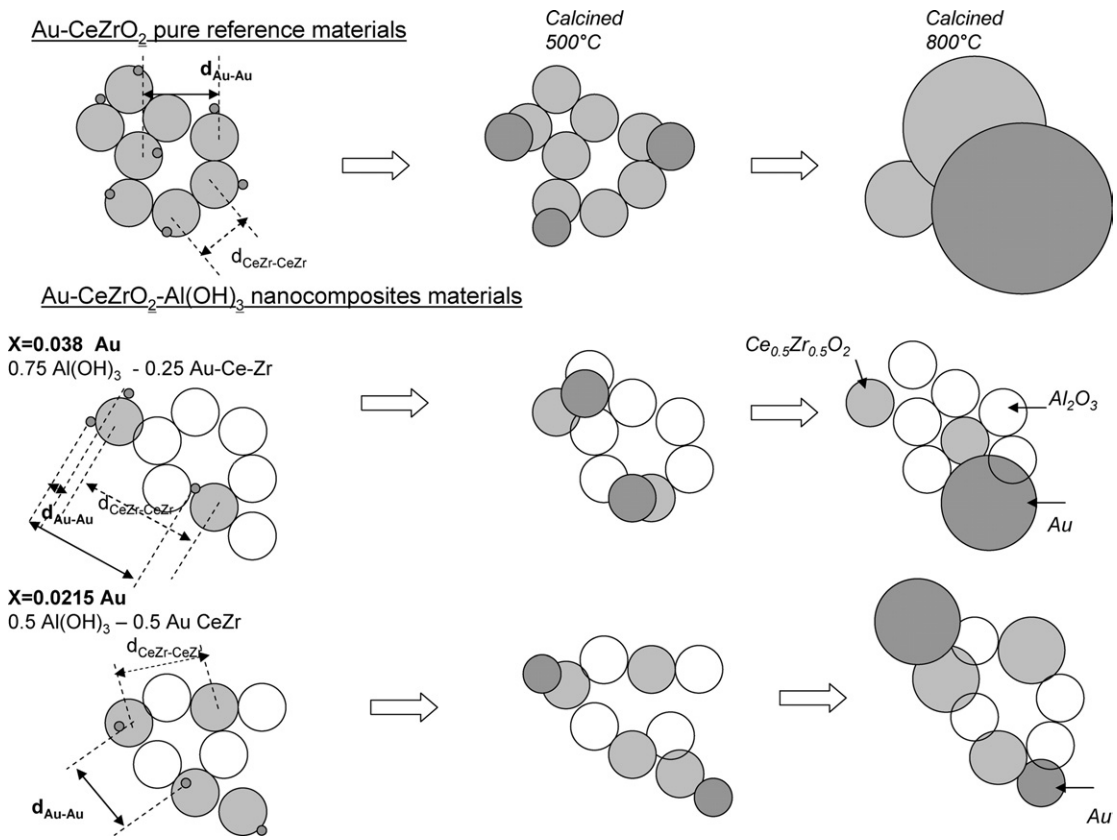

Fig. 8 Schematic representation of Au–$Ce_{0.5}Zr_{0.5}O_2$–$Al(OH)_3$ nanostructured materials prepared by assembling nanoparticle building blocks and displaying similar Au content but different $d_{CeZr-CeZr}$ and d_{Au-Au} values. Au–$Ce_{0.5}Zr_{0.5}O_2$–$Al(OH)_3$ nanocomposites displaying similar *y*Au wt content, $y = 0.75$, 1.0 and 1.5%, were prepared using mixtures involving $Al(OH)_3$ colloids in appropriate proportions and formulated with *x*Au–$Ce_{0.5}Zr_{0.5}O_2$ colloids displaying various *x* Au wt contents, $0.002 < x < 0.05$. Reported dimensions for Au particles and $Ce_{0.5}Zr_{0.5}O_2$ grain sizes were adjusted from TEM pictures observations.

described for the synthesis of pure $Ce_{0.5}Zr_{0.5}O_2$ colloids.[29] Typically, 34.375 g $(NH_4)_2Ce(NO_3)_6$, 2.1 g $Ce(NO_3)_3{\cdot}6H_2O$, 14.585 g $ZrO(NO_3)_2$, 1.8 g $HAuCl_4{\cdot}xH_2O$, 52 Au wt% were dissolved in HNO_3 solution. The reaction mixture had a total volume of 1000 ml and a $H^+/Ce(IV)$ molar ratio of 0.5. Co-precipitation of the Au and metal hydroxides was achieved at pH 10 by instantaneous addition of 90 ml of 30% NH_3 solution. The precipitate was washed repeatedly with purified water and re-dispersion was achieved by acetic acid addition. The resulted suspensions were aged under stirring at room temperature with daylight exposure for 5 days allowing Au(III) partial reduction. Stable colloidal dispersions were achieved after maintaining the dispersions in an oven at 60 °C for 24 h without stirring. Removal of residual ionic species or Au clusters non-attached to Au–$Ce_{0.5}Zr_{0.5}O_2$ colloids smaller than 2 nm was achieved by washing thoroughly by 6 volumes of distilled H_2O using an ultra filtration cell equipped with 3kDa membranes. Thus, 200 ml of transparent coloured 0.45 M Au–$Ce_{0.5}Zr_{0.5}O_2$ dispersions were obtained, which were stable with respect to precipitation for more than six months. Chemical analysis performed on these dispersions gave $(Ce/Zr)_{molar} \sim 1$ and $(Au/Ce_{0.5}Zr_{0.5}O_2)_{wt} = 0.0215$. UV-Vis spectra were acquired in the 800 to 200 nm wavelength range on as-prepared and after centrifugation of 5× diluted samples in quartz cells (1 cm path length) using a Perkin Elmer Lambda 16 ultraviolet-visible spectrophotometer.

5 nm spherical $Al(OH)_3$ colloids were prepared by controlled hydrolysis of $AlCl_3$ solution using thermal decomposition of urea.[30] Transparent $Al(OH)_3$ colloidal dispersions were obtained by HNO_3 redispersion. Dispersions were purified by ultrafiltration, as previously described, before use. Various Au–$Ce_{0.5}Zr_{0.5}O_2$–Al_2O_3 nanocomposites were prepared at a constant global Au content ($y = 0.75$, 1 and 1.5 Au wt%) using Au–$Ce_{0.5}Zr_{0.5}O_2$ colloidal dispersions displaying Au contents ranging from $x = 0.002$ to 0.05 by mixing appropriate ratios of $Al(OH)_3$ colloidal dispersion at pH 4. The $Ce_{0.5}Zr_{0.5}O_2$ volume fraction of the nanocomposites varied from 0.25 to 0.5. Solid nanocomposite samples, obtained by evaporation of the water at room temperature in air, were dried for 6 h at 200 °C. The dried powders were re-dispersed at room temperature under vigorous stirring in NH_3 solution at pH 10. The solid was then isolated by filtration and washed until free of chloride. Calcination was performed in air at two different temperatures (500 and 800 °C) for 6 h.

Specific surface area and pore size distributions were determined from N_2 adsorption isotherms recorded with an ASAP 2010 M micrometer. Samples were out-gassed at 300 °C for 3 h before analysis. Crystal domain sizes ($L_{(hkl)}$) along the c and a axes were calculated from the (002) and (310) planes, respectively, applying Scherrer's formula, $L_{(hkl)} = 0.94\lambda[(\cos\theta)\sqrt{(\Delta_r^2 - \Delta_0^2)}]^{-1}$ where θ is the diffraction angle for the hkl plane, Δ_r and Δ_0 the widths in radians of the hkl reflexion at half height for the as-synthesized and reference materials, respectively ($\lambda = 1.5405$ Å). A Jeol Jem 2100F transmission electron microscope with an accelerating voltage of 200 kV, equipped with an Energy Dispersive Spectrometer EDS (probe surface of 5.0 nm × 5.0 nm) was used to study the Au distribution within the Au–$Ce_{0.5}Zr_{0.5}O_2$ nanoparticles or in the calcined Au–$Ce_{0.5}Zr_{0.5}O_2$–Al_2O_3 nanocomposites.

CO conversion was measured in a tubular plug-flow reactor as a function of temperature between 20 and 200 °C on calcined nanocomposites. A preliminary reduction step under 10% (vol.) H_2 in Ar at 300 °C for one hour, was carried out before the catalytic test. The standard test used a 110 cm^3 min^{-1} reactant flow with $(CO : O_2 : Ar)_{molar} = (1.0 : 0.6 : 98.4)$ and a contact time (W/F) of 34 g_{cat} h $mol_{CO^{-1}}$.

References

1 N. Chandrasekharan and P. V. Kamat, *J. Phys. Chem. B*, 2000, **104**, 10851.
2 M. Haruta, N. Yamada, T. Kobayashi and S. Ijima, *J. Catal.*, 1989, **115**, 301.
3 M. Haruta, *Catal. Today*, 1997, **36**, 153.
4 P. Landom, J. Ferguson, B. E. Solsom, T. Garcia, S. Al Sayari, A. F. Carley, A. A. Herzing, C. J. Kiely, M. Makkee, J. A. Mouljiu, A. Overweg, S. F. Golunski and G. J. Hutchings, *J. Mater. Chem.*, 2006, **16**, 199.
5 J. K. Edwards, B. E. Solsona, P. Landon, A. F. Carley, A. Herzing, C. J. Kiely and G. J. Hutchings, *J. Catal.*, 2005, **236**, 69.
6 W. D. Provine, P. L. Mills and J. J. Lerou, *Stud. Surf. Sci. Catal.*, 1996, **101**, 191.
7 Patent application, *Eur Pat.* 0654301, BP Chemicals, 1994.
8 S. Kielbassa, M. Kinne and R. J. Bohm, *J. Phys. Chem. B*, 2004, **108**, 19184.
9 C. W. Corti, R. J. Holliday and D. T. Thompson, *Appl. Catal., A: General*, 2005, **293**, 253.
10 G. Patrick, E. Van der Lingen, C. W. Corti, R. J. Holliday and D. T. Thompson, *Top. Catal.*, 2004, **30-31**, 273.
11 C. E. Mitchell., A. Howard, M. Carney and R. G. Egdell, *Surf. Sci.*, 2001, **490**, 196.
12 T. A. Nijhuis, B. J. Huizinga, M. Makkee and J. A. Moulijn, *Ind. Eng. Chem. Res.*, 1999, **38**, 884.
13 P. M. Arnal, M. Comotti and F. Schulth, *Angew. Chem., Int. Ed.*, 2006, **15**, 8224.
14 K. Yu, Z. Wu, Q. Zhan, B. Li and X. Xie, *Phys. Chem. C*, 2008, **112**, 2244.
15 M. P. Casaletto, A. Longo, A. Martorana, A. Prestianni and A. M. Venezia, *Surf. Interface Anal.*, 2006, **38**, 215.
16 M. S. Chen and D. W. Goodman, *Science*, 2004, **306**, 252.
17 J. A. Rodriguez, X. Wang, P. Liu, W. Wen, J. C. Hanson, J. Hrbek, M. Perez and J. Evans, *Top. Catal.*, 2007, **44**(1-2), 73.
18 S. Carriettin, P. Concepcion, A. Corma, J. M. Lopez-Nieto and V. F. Puntes, *Angew. Chem., Int. Ed.*, 2004, **43**, 2538.
19 L. L. Murrell and S. J. Tauster, in *Studies in Surface Science and Catalysis: Catalysis and Automotive Pollution Control II*, ed. A. Cruq, Elsevier, Amsterdam, 1991, vol. 71, p. 547.
20 M. H. Yao, R. J. Baird, F. W. Kunz and T. E. Hoost, *J. Catal.*, 1997, **166**, 67.
21 Q. Long, M. Cai, J. D. Rogers, H. Rong, J. Li and L. Jiang, *Nanotechnology*, 2007, **18**, 355601.
22 M. Fernandez-Garcia, A. Martinez-Arias, A. Iglesias-Juez, C. Belver, A. B. Hungria, J. C. Conesa and J. Soria, *J. Catal.*, 2000, **194**, 385.
23 T. Soejima, H. Tada, T. Kawahara and S. Ito, *Langmuir*, 2002, **18**, 4191.
24 M. C. Daniel and D. Astruc, *Chem. Rev.*, 2004, **104**(1), 293.
25 D. G. Duff, A. Baikar and P. P. Edwards, *Langmuir*, 1993, **9**, 2301.
26 M. Brust, M. Walker, D. Bethell, D. J. Schiffrin and R. Whyman, *J. Chem. Soc., Chem. Commun.*, 1994, 801.
27 T. Akita, M. Okumura, K. Tanaka, M. Kohyama and M. Haruta, *Catal. Today*, 2006, **117**, 62.
28 J. Y. Chane-Ching, M. Airiau, A. Sahibed-dine, M. Daturi, E. Brendle, F. Ozil, A. Thorel and A. Corma, *Langmuir*, 2004, **21**, 1568.
29 A. S. Deshpande, N. Pinna, P. Beato, M. Antonietti and M. Niederberger, *Chem. Mater.*, 2004, **16**, 2599.
30 N. I. Kandri, A. Ayral, C. Guizard, H. El Ghadraoui and L. Cot, *Mater. Lett.*, 1999, **40**, 52.